University of Massachusetts Amherst

From the SelectedWorks of Jennifer Ross

May, 2008

Complementary dimerization of microtubule-associated protein tau: Implications for microtubule bundling and tau-mediated pathogensis

Jennifer Ross, *University of Massachusetts - Amherst*
Kenneth J Rosenberg
H. Eric Feinstein
Stuart C Feinstein
Jacob Israelachvili

Available at: https://works.bepress.com/jennifer_ross/6/

Complementary dimerization of microtubule-associated tau protein: Implications for microtubule bundling and tau-mediated pathogenesis

Kenneth J. Rosenberg*, Jennifer L. Ross†, H. Eric Feinstein‡, Stuart C. Feinstein‡, and Jacob Israelachvili§¶

*Department of Physics, ‡Neuroscience Research Institute and Department of Molecular, Cellular, and Developmental Biology, and §Department of Chemical Engineering and Materials Department, University of California, Santa Barbara, CA 93106; and †Department of Physics, University of Massachusetts, Amherst, MA 01003

Contributed by Jacob Israelachvili, March 4, 2008 (sent for review December 17, 2007)

Tau is an intrinsically unstructured microtubule (MT)-associated protein capable of binding to and organizing MTs into evenly spaced parallel assemblies known as "MT bundles." How tau achieves MT bundling is enigmatic because each tau molecule possesses only one MT-binding region. To dissect this complex behavior, we have used a surface forces apparatus to measure the interaction forces of the six CNS tau isoforms when bound to mica substrates *in vitro*. Two types of measurements were performed for each isoform: symmetric configuration experiments measured the interactions between two tau-coated mica surfaces, whereas "asymmetric" experiments examined tau-coated surfaces interacting with a smooth bare mica surface. Depending on the configuration (of which there were 12), the forces were weakly adhesive, strongly adhesive, or purely repulsive. The equilibrium spacing was determined mainly by the length of the tau projection domain, in contrast to the adhesion force/energy, which was determined by the number of repeats in the MT-binding region. Taken together, the data are incompatible with tau acting as a monomer; rather, they indicate that two tau molecules associate in an antiparallel configuration held together by an electrostatic "zipper" of complementary salt bridges composed of the N-terminal and central regions of each tau monomer, with the C-terminal MT-binding regions extending outward from each end of the dimeric backbone. This tau dimer determines the length and strength of the linker holding two MTs together and could be the fundamental structural unit of tau, underlying both its normal and pathological action.

bridging interaction | intrinsically unstructured proteins | protein dimerization | surface forces | bioadhesion

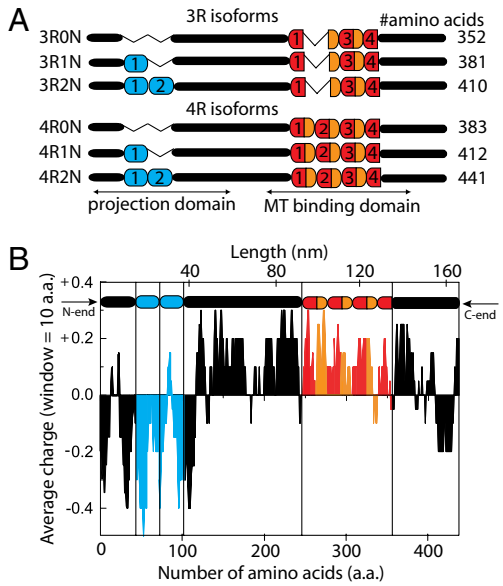

Fig. 1. A schematic of the six CNS tau isoforms, with their associated charge distributions. (*A*) The six isoforms, generated by alternative RNA splicing, differ by the presence of either three or four 18-aa-long imperfect repeats (red), separated from one another by a 13-to 14-aa interrepeat (orange), in the C-terminal half of the protein and the presence of zero, one, or two 29-aa inserts in the N-terminal half of the protein. (*B*) Charge-distribution plot (using 10-aa windows) shows that the N terminus is negatively charged and the C terminus is positively charged.

The neural microtubule (MT)-associated protein (MAP) tau is essential for the proper development and maintenance of the nervous system. Among other functions, tau promotes the assembly of MTs into well organized, evenly spaced bundles in neuronal axons (1–6) and regulates the growing and shortening dynamics of individual MTs (7–11). Tau dysfunction has long been correlated with many neurodegenerative diseases, including Alzheimer's and related dementias. In the past decade, mutational analyses have demonstrated a direct cause-and-effect relationship between tau dysfunction and/or misregulation and the dramatic neuronal cell death underlying many of these dementias [for example, FTDP-17 (12–14)]. Some mutations cause amino acid substitutions in tau, whereas others are regulatory, causing aberrant patterns of tau RNA splicing without affecting the tau amino acid sequence.

As a result of alternative RNA splicing, there are six naturally occurring isoforms of tau expressed in the CNS (Fig. 1). Based on sequence analysis and structure–function dissection (5, 8, 9, 15–18), tau can be viewed as possessing four distinct regions. The C-terminal tail contains both basic and acidic subregions and serves to indirectly regulate tau binding to MTs, at least in part via regulated phosphorylation. On the N-terminal side of this tail is the MT-binding region, which is composed of either three or four imperfect repeats (18 aa in length) separated from one another by interrepeats (13–14 aa in length). The repeat/interrepeat region is positively charged, which is widely believed to facilitate electrostatic interactions between tau and the negatively charged MT surface (19–21). The presence or absence of the interrepeat between repeats 1 and 2 and the second repeat distinguishes three-repeat tau (3R) from four-repeat tau (4R) (22). On the N-terminal side of the MT-binding region resides a very positively charged proline-rich region that harbors many sites of phosphorylation and serves to indirectly regulate the

Author contributions: K.J.R., J.L.R., H.E.F., S.C.F., and J.I. designed research; K.J.R. and J.I. performed research; J.L.R., H.E.F., and S.C.F. contributed new reagents/analytic tools; K.J.R., J.L.R., H.E.F., S.C.F., and J.I. analyzed data; and K.J.R., J.L.R., H.E.F., S.C.F., and J.I. wrote the paper.

The authors declare no conflict of interest.

¶To whom correspondence should be addressed. E-mail: jacob@engineering.ucsb.edu.

This article contains supporting information online at www.pnas.org/cgi/content/full/0802036105/DCSupplemental.

© 2008 by The National Academy of Sciences of the USA

ability of the MT-binding region to associate with MTs (5, 8, 9). Finally, the N-terminal region of the protein is negatively charged and contains zero, one, or two negatively charged inserts (29 aa each), again determined by alternative RNA splicing. Together, the N terminus and the proline-rich region constitute the ''projection domain,'' which is believed to extend outward from the MT surface and to determine the inter-MT distance in MT bundles (2).

Tau isoform expression patterns are tightly regulated. Fetal human brain expresses only 3R tau, whereas adult brain expresses approximately equal amounts of 3R and 4R tau (22–24). Regulatory mutations that alter the adult brain tau isoform expression profile to ≈75% 4R tau and ≈25% 3R tau (without changing the amino acid sequence) cause extensive neuronal cell death and dementia in diseases such as FTDP-17 (12, 14). That altered expression ratios of otherwise normal tau proteins lead to such dramatic consequences demonstrates that functional differences must exist between 3R and 4R tau. Indeed, 4R tau binds to MTs with a greater affinity than 3R tau by a factor of approximately three (6, 17, 25), and it is a more potent regulator of MT dynamics than is 3R tau (8, 10, 11, 26). Qualitative differences between 4R tau and 3R tau have also been described (11, 18). In contrast, relatively little is known about the effects of the N-terminal end insertions. The N-terminal region is known to mediate tau's association with the plasma membrane (27) and to influence MT nucleation (5). Additional work also suggests that the N-terminal inserts may affect the efficacy of tau as a substrate for some kinases (28).

Tau has long been viewed as an ''unstructured'' protein because it lacks significant secondary structure (29–33), at least when not associated with MTs. This property is especially important in trying to understand the structural basis of tau function because previous studies have suggested that the unstructured ''projection domain'' may be a key element in determining the spacing of MTs in tau-induced MT bundles (2, 34). More specifically, although the molecular basis of its action is unclear, tau can organize MTs into parallel and uniformly spaced assemblies known as MT bundles in axons, despite the fact that each tau molecule possesses only one MT-binding region. In this regard, Hoh and coworkers (35, 36) suggested that tau and other MT-associated proteins may form a brush-like layer on the outer surface of MTs and arrange the MT network entirely via steric hindrance within a defined volume arising from tau's projection domain, similar to the entropic repulsion from a ''polymer brush.'' Mandelkow and colleagues (37) proposed a model of tau as a flexible or compressible spacer that acts to keep MTs from forming a closely packed array, based on x-ray scattering data. Others have speculated that tau and other MAPs can form cross-bridges either through attractive protein–protein interactions or through direct bridging of tau to a neighboring MT (2, 38, 39).

To gain a better understanding of the tau structure–function relationship, we used a surface forces apparatus (SFA) to determine the force profile for each of the six tau isoforms physisorbed through self-assembly from solution to negatively charged mica surfaces. Mica has a charge density similar to that of the outer surface of a MT (≈1 e^-/nm^2) (40, 41) and therefore may approximate the electrostatic nature of MT surfaces. In some experiments, two tau-coated mica surfaces were brought into contact to approximate the interactions between two tau-coated MTs (''symmetric'' experimental configuration). In other experiments, one tau-coated and one bare mica surface were brought together to approximate the interactions between a tau-coated MT and an ''undecorated'' MT (''asymmetric'' experimental configuration). All six tau isoforms were studied to define the interaction properties of each and thereby determine which parts of the protein participate in various aspects of tau function. Taken together with the biological capabilities of tau, the data suggest a model in which tau forms antiparallel dimers, held together by an electrostatic zipper consisting of multiple complementary binding sites or salt bridges.

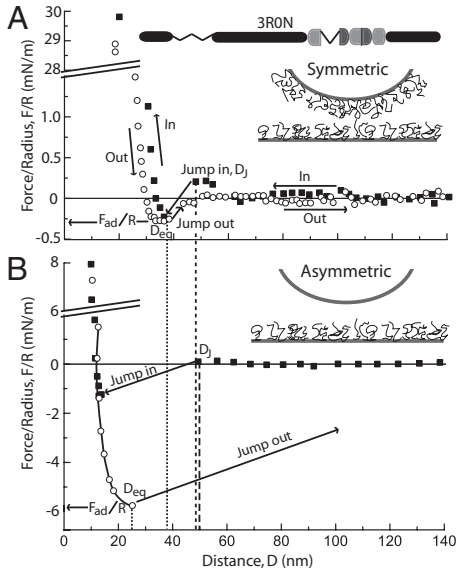

Fig. 2. Force data for the 3R0N tau isoform. (*A*) Symmetric configuration. (*B*) Asymmetric configuration. For each, the force F is normalized by the radius of curvature of the mica surfaces R and plotted versus the surface separation distance D. Filled squares and ''In'' curve: forces measured between approaching surfaces; open circles and ''Out'' curve: forces measured between receding surfaces. There are two instabilities where surfaces spontaneously jump in or out: D_J is the jump-in separation, which gives the ''range'' of the interaction, and D_{eq} is the jump-out separation, which gives the ''equilibrium'' configuration and lowest (binding) energy, $E_{eq} = F_{ad}/2\pi R$.

Results

Force–Distance Profiles. By using the SFA, the normal force F can be measured as a function of the closest distance D between the cylindrically curved mica substrates each of radius R [see supporting information (SI) *Text* for details]. By using the Derjaguin approximation (41), one can show that for the crossed-cylinder geometry used in the SFA, the measured force vs. distance $F(D)$ between two cylindrically curved surfaces is related to the interaction energy per unit area $E(D)$ between two flat surfaces by $F(D)/R = 2\pi E(D)$. Thus, normalized force plots of F/R vs. D reflect the interaction energy between two planar surfaces mediated by tau. We performed both symmetric and asymmetric SFA experiments for all six tau isoforms, i.e., 12 different configurations in all.

Data for the shortest tau isoform, possessing three repeats and zero projection-domain inserts and denoted 3R0N, is shown in Fig. 2. The other five isoforms displayed qualitatively similar force curves (see Figs. S1–S6), and a graphical summary of the quantitative differences is presented in Fig. 3. These interactions and their differences will now be described.

For the 3R0N isoform in the symmetric configuration (Fig. 2*A*), no force was detected at large distances ($D > 60$ nm, black squares). As the surfaces were brought together, a weak repulsion at approximately $D = 55$ nm was followed by a weak attraction as the surfaces spontaneously ''jumped in'' from $D_J = 49 \pm 1$ nm to $D \approx 35$ nm. Further compression revealed a steep repulsion (In curve). On retracting the surfaces (Out curve) the surfaces jump out from $D_{eq} = 38 \pm 2$ nm.

The force profile for 3R0N tau in the asymmetric configuration is shown Fig. 2*B*. A number of similarities and differences between the two systems are immediately apparent. First, no

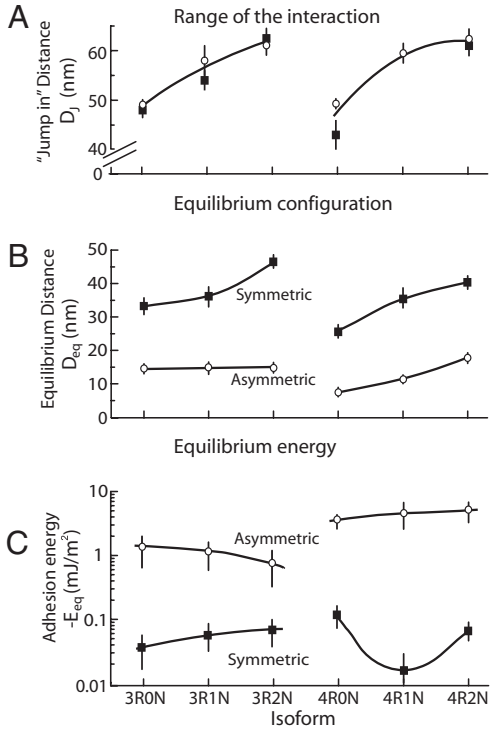

Fig. 3. Characteristic ranges of the binding interactions (given by D_J) and magnitudes of the adhesion energies (given by $E_{eq} = F_{ad}/2\pi R$) for the 12 configurations studied.

repulsive force is detected upon approach in the asymmetric configuration. Quite remarkably, however, the surfaces in the asymmetric configuration jump in at exactly the same separation distance, $D_J = 49 \pm 2$ nm, as in the symmetric configuration. Upon further compression, the minimum separation in the asymmetric experiment ($D \approx 10$ nm) is approximately half that in the symmetric case ($D \approx 20$ nm), as expected, and the equilibrium separation at $D_{eq} = 26 \pm 2$ nm is less than for the corresponding symmetric configuration. Interestingly, the adhesion energy measured in the asymmetric configuration ($E_{eq} = F_{ad}/2\pi R = 1.2 \pm 0.6$ mJ/m^2) is well over an order of magnitude larger than in the symmetric configuration ($E_{eq} = 0.04 \pm 0.02$ mJ/m^2).

The jump-in distances D_J, the equilibrium separation distances D_{eq}, and the adhesion or binding energies E_{eq} for the six tau isoforms in both the symmetric and asymmetric configurations are plotted graphically in Fig. 3. Fig. 3*A* shows that for any given isoform, the range of the interaction D_J is the same regardless of whether the configuration is symmetric or asymmetric. However, although D_J is not affected by the number of C-terminal imperfect repeats, it increases as a function of increasing number of N-terminal projection-domain inserts. With respect to the equilibrium separation distances, Fig. 3*B* shows that for any given isoform, D_{eq} is always larger in the symmetric than the asymmetric case. Additionally, increasing the number of projection domain inserts often increases D_{eq}, but adding a fourth repeat generally decreases D_{eq}. The most dramatic observation is with respect to adhesion energies (Fig. 3*C*) showing that (*i*) for all isoforms, they are always at least an order of magnitude greater in the asymmetric configuration, and (*ii*) in the asymmetric case, E_{eq} is higher for isoforms with four repeats than for those with three, whereas the number of projection-domain inserts has no significant effect on the values of E_{eq}. The apparently anomalous minimum in the adhesion of the symmetric 4R1N isoform seemingly poses a challenge.

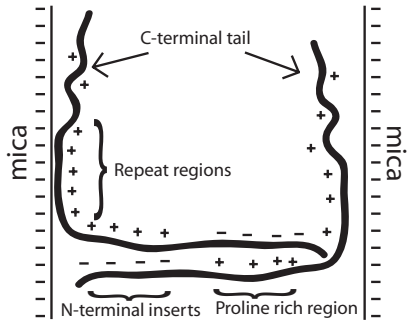

Fig. 4. Cartoon model of bivalent tau dimer held together by an electrostatic zipper and interacting with two mica (model MT) surfaces.

However, we note that the 1N isoforms in the projection domains have the highest negative charge density (Fig. 1*B*), which would act to reduce their overall adhesion (due to van der Waals, H-bonding and/or hydrophobic interactions) more than in the case of the 0N and 2N domains. Within the error of our measurements (Fig. 3*C*), it is also possible that the 3R isoforms show the same behavior although the subtle discrepancies in their adhesions were too small to measure accurately enough to establish this unambiguously.

Adsorbed Mass Measurements. Measurements of the surface-adsorbed density of tau provided further insights into the nature of the self-assembled layers of tau. The average adsorbed mass density for each of the six isoforms was calculated by using a refractive index method used in conjunction with the interferometric analysis of the SFA (see *Materials and Methods* and *SI Text*). If a monolayer of tau is assumed to be present on each mica surface, then on average, each tau protein occupies an area of ≈ 8 nm^2, or <3 nm between neighboring tau molecules. Because the expected radius of gyration R_g of tau is ≈ 6 nm (42), this spacing is too small to accommodate a tau monolayer. Instead, this high density of tau points to the presence of dimers (and possibly higher-order oligomers) on the surfaces.

Discussion

Dimerization of Tau Provides a Simple Explanation for the SFA Results, a Molecular Mechanism for Tau-Mediated MT Bundling, and Perspectives on Pathological Tau Action. Our initial expectation was that the positively charged proline-rich and repeat/interepeat regions of tau would adhere well to the negatively charged mica surface, with the negatively charged N terminus of tau extending outward. We also anticipated that the only forces that would be observed as this negatively charged N-terminal region of tau approached either (*i*) a non-tau-treated, negatively charged mica surface in the asymmetric experimental configuration or (*ii*) negatively charged tau tails projecting outward from the other mica surface in the symmetric experimental configuration would be repulsive. It was therefore surprising to observe a strongly attractive interaction in both the symmetric and asymmetric experimental configurations. Taken together with the adsorbed mass data, the simplest interpretation suggests that the tau structures in the experiment possess two mica-binding sites, separated from one another by a maximum of 50 nm (the D_J for 3R0N and 4R0N). Given the charge distribution of individual tau molecules (Fig. 1), we propose that tau forms stable dimers in solution, held together by a complementary electrostatic zipper between the positively charged proline domain of each constituent monomer and the negatively charged N-terminal tail of its partner molecule (Fig. 4). Because these dimers form before adsorption on mica, the positively charged proline-rich region contained in this zipper is already complexed in the dimer and

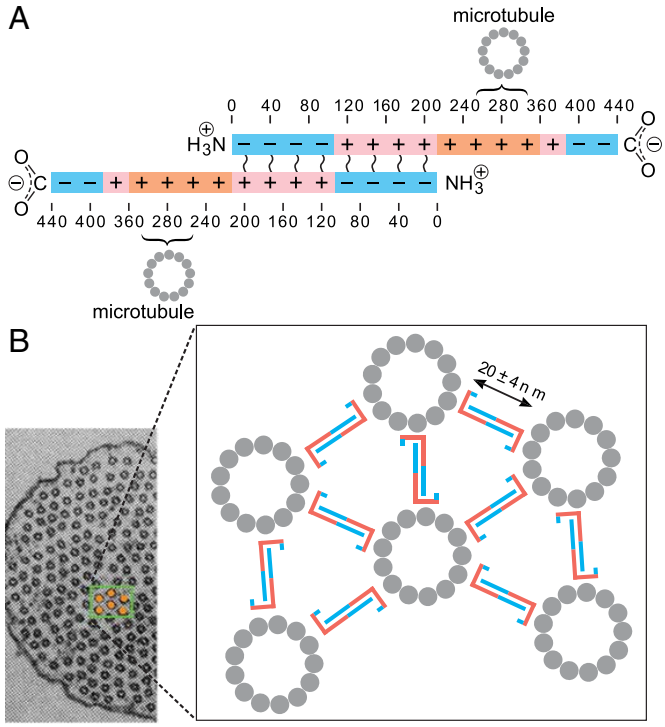

Fig. 5. Cartoon model of bivalent tau dimer associating with and bundling MTs. (*A*) The amino acid proposed to form the electrostatic zipper is emphasized. (*B*) Bivalent tau dimers bundling MTs is depicted. The electron micrograph of bundled MTs is from ref. 2 [adapted by permission from Macmillan Publishers Ltd: *Nature* (2), copyright 1992].

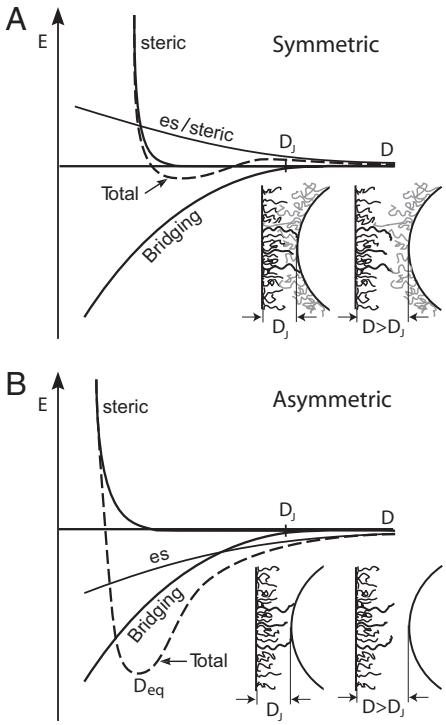

Fig. 6. The total interaction energy *E* decomposed into the fundamental steric, electrostatic (es), and mica–mica bridging forces for the symmetric (*A*) and asymmetric (*B*) cases. The tau molecules in bold are those involved in a bridging interaction.

is thus unable to bind to mica. This proposed zipper is in many ways similar to the zipper structure underlying homophilic *N*-cadherin dimerization (43–45), which promotes cell–cell adhesion. The "bivalent" tau structure thus possesses a dimerized central core with a positively charged C-terminal MT-binding region extending from each of its ends.

Tau dimers/oligomers have been described previously (46–51), focusing primarily on intermolecular dimerization mediated by disulfide bonds: 3R tau has a single cysteine residue, whereas 4R tau has two cysteines. Most of this earlier work also focuses on dimerization as a possible nucleation mechanism for pathological tau aggregation. However, it is very unlikely that disulfide bonds could form in the reducing environment present in normal neuronal axoplasm. Additionally, we believe that disulfide bond-mediated dimerization is very unlikely in this system. First, because 4R tau possesses two cysteines (one in repeat 2 and the other in repeat 3), intra- rather than intermolecular bonding would be most likely. In this case, tau would be frozen in a monomeric state, and the observed attractive force would not exist. Second, in the event that intermolecular disulfide bonds did form with either 3R or 4R tau, this would link the two molecules within their positively charged repeat–interrepeat regions, which would adhere to the mica surface), leaving two negatively charged N-terminal tails extending outward from the mica. Again, this structure would exhibit only repulsion and not attraction.

This again raises the question of how tau, possessing only one MT-binding region per molecule, could lead to the uniform spacing of MTs observed in axonal MT bundles. Consistent with the notion of tau dimers, quick-freeze, deep-etch electron microscopy has revealed tau cross-bridges making contact between adjacent MTs in bundles (2). Additionally, biochemical data have been presented demonstrating disulfide-independent tau dimerization and higher-order oligomerization (50), although molecular mechanisms were not suggested. If correct, the proposed electrostatic tau zipper model provides a simple mechanism to account for these observations and the phenomena of MT bundling (Fig. 5 *A* and *B*). The lengths of observed cross-bridges in tau containing cells is typically in the range of 20–27 nm (2). Quantitative application of our force data to MTs requires knowledge of the radius of the MTs, the density of tau on the MT surface, and whether all of the taus bind radially out as illustrated in Fig. 5*B* or also at non-90° angles to the MT surfaces. In the latter case the (smaller) D values at $F = 0$ rather than at F_{ad} should be compared with the electron micrograph values. Taking the full range of possible D values from the force–distance data in the symmetrical configurations shown in Fig. 2, Figs. S1–S3, and Fig. S5, we obtain 23–38 nm, which overlaps the observed range of 20–27 nm.

A charge-distribution analysis of the N-terminal region of MAP2 (which is much longer than the N-terminal region of tau) suggests that it might also be able to dimerize, consistent with greater inter-MT distance in MAP2-promoted MT bundles.

Finally, the location of the zipper coincides with the neurotoxic 17-kDa proteolytic fragment of tau generated after Aβ treatment of hippocampal cells (52). We propose that the 17-kDa fragment exerts its toxicity by acting as a competitive inhibitor of tau dimerization, which we propose could be essential for tau function. Indeed, tau fragments containing the MT-binding region but lacking the N terminus have severely compromised functional capabilities (9, 11). Additionally, many tau phosphorylation sites reside within the zipper region, and these could affect normal and pathological tau action by altering the complementarity of the electrostatic interactions underlying tau dimerization.

Tau Structure and Function

Tau–Mica Bridging Distance Depends on the Projection Domain Length. The jump-in distance D_J is the same in the symmetric and asymmetric experiments for each of the six tau isoforms (Fig. 3*A*).

For the asymmetric configuration, the simplest interpretation of these observations is that this is the distance at which tau dimers from one mica surface first make contact with the second mica surface. For the symmetric configuration, the simplest interpretation of these observations is that as tau dimers approach one another, they interdigitate, eventually making contact with both mica surfaces. Thus, D_J can be thought of as corresponding to the height of the tau dimers on a mica surface. We also observe that D_J depends on the number of N-terminal insertions within the projection domain but has no dependence on the number of C-terminal repeats (Fig. 4*A*). This observation is consistent with the current picture of tau structure-function in which the C-terminal region binds directly to MTs (53, 54), whereas the N-terminal projection domain extends away from the MT surface.

Equilibrium Separation Distances D_{eq} Depend on the Projection-Domain Length. In Fig. 3*B*, the equilibrium separation distance is plotted for each tau isoform. The data indicate that D_{eq} is larger in the symmetric configuration than in the asymmetric one. This difference is likely because of the presence of an additional steric repulsion due to tau–tau interactions (discussed below in *Analysis of Force Curves*). This would cause a shift of D_{eq} to larger distances while also reducing the E_{eq}, which was also observed. Additionally, the data reveal that D_{eq} generally increases with the number of N-terminal inserts (with the exception of 3R tau in the asymmetric configuration), consistent with their presence in the projection domain.

Adhesion Energy Depends on Mica Availability and the Number of MT-Binding Repeats. The asymmetric experiments consistently show increased adhesion energy over the symmetric experiments by at least an order of magnitude (Fig. 3*A*). This is not surprising because the available binding area is much larger for a bare mica surface compared with a surface that has a layer of adsorbed tau dimers on it. In the symmetric configuration, it may well be that only a small fraction of the tau dimers originally adhering to one surface are actually successful at reaching the other mica surface. In addition, the presence of the negatively charged N-terminal inserts plays no significant role in binding of tau to mica. Finally, the 4R isoforms adhere approximately five times greater than the 3R isoforms in the asymmetric configuration, consistent with the well established fact that 4R tau binds to MTs with ≈3-fold greater affinity than does 3R tau (6, 8, 25).

Analysis of Force Curves. Comparing the force profiles of the six different isoforms in both the symmetric and asymmetric configurations allows us to determine the different force contributions to the overall interaction. As illustrated in Fig. 6, a combination of repulsive steric, attractive and repulsive electrostatic, and attractive tau–mica bridging interactions together give rise to the net (measured) force profile. For example, in the symmetric case (Fig. 6*A*), the short-range steric interaction begins at a distance that is twice that of the asymmetric case, as expected because of the second tau surface. Meanwhile, the attractive tau–mica bridging interaction, which is responsible for the observed jump in, occurs at the same tau layer height for both the symmetric and asymmetric cases. Additionally, the symmetric configuration is expected to have an additional long-range repulsive interaction because of the electrostatic or steric contribution arising from the overlap between the tau layers at distances slightly larger than D_J. This repulsion would not only be absent in the asymmetric case, but a slightly attractive electrostatic force might be expected as the negatively charged mica surface approaches the positively charged tau-covered mica surface.

When the curves of these individual forces are combined, the resultant interaction curves (i.e., repulsive steric tau–tau interaction and attractive electrostatic tau–mica interaction), when combined, reproduce many of the significant observations of the forces curves (compare Fig. 6 with Fig. 3). In particular, this explains why the force curve starts further away in the symmetric case and why D_J is the same for both configurations. Also, the schematic drawings of the two surfaces explain why the hysteresis, or difference between receding and approaching force curves, is much larger for the asymmetric configuration. Unlike in the symmetric case, not only is there no barrier to reaching the opposite mica, but the sheer availability of binding sites on the mica is much greater in the asymmetric configuration, which allows for considerably greater adhesion between tau and the opposing mica surface.

Materials and Methods

SFA Measurements. A SFA III was used to measure the interaction forces (41). Briefly, two molecularly smooth mica surfaces (2- to 4-μm thick) were glued onto hemicylindrical (radius $R \approx 1$ cm) silica substrates. The backside of each mica piece had a semireflecting silver coating to allow for multiple reflections of the light beam. The surfaces were arranged with their cylindrical axes perpendicular to each other. The force was measured by determining the deflection ΔD of the spring supporting the lower surface ($F = -k\Delta D$, spring constant = k) with a resolution of $\pm$ 1 Å in distance from the ''fringes of equal chromatic order'' (FECO) pattern generated by using multiple-beam interferometry. To normalize the force F between positions with different local radii R, the force was divided by the local radius R at each position. All distances D are relative to the two mica surfaces in molecular contact ($D = 0$). Forces with a positive sign are repulsive, and forces with a negative sign are attractive.

Recombinant tau was purified as described in ref. 11. Tau concentrations were determined by SDS/PAGE comparison with a 3R tau mass standard (10). Each purified tau sample was diluted to 0.2 mg/ml in 1 mM K-Pipes [1 mM Pipes, 2.7 mM KOH (pH = 6.8)]. The low ionic strength was used to ensure strong electrostatic binding between tau and mica. Before use, tau was briefly warmed to 90°C and centrifuged at top speed in a microfuge for 15 min. To prepare a tau-coated mica surface, 10 μl of the tau solution was placed on the surface for 10 minutes. Next, the surface was gently rinsed with >5 ml of 1 mM K-Pipes to wash off weakly and nonadsorbing tau. The surfaces were returned into the SFA, ensuring that a liquid lens of buffer remained on top of the tau-coated mica surface at all times. Once secure, the SFA was completely filled (total volume ≈80 ml) with buffer. Finally, the SFA was allowed to thermally equilibrate ($T = 25.0 \pm 0.1$°C) before measurements were taken. Additional SFA information is available in *SI Text*.

ACKNOWLEDGMENTS. We thank Michelle Gaylord (University of California, Santa Barbara) for providing some of the tau samples. This work was supported by a grant from the Institute for Collaborative Biotechnologies at the University of California, Santa Barbara (to J.I.) and National Institutes of Health Grant R01 NS 35010 (to S.C.F.).

1. Chapin S, Bulinski J, Gundersen G (1991) Microtubule bundling in cells. *Nature* 349:24.
2. Chen J, Kanai Y, Cowan N, Hirokawa N (1992) Projection domains of Map2 and tau determine spacings between microtubules in dendrites and axons. *Nature* 360:674–676.
3. Scott CW, *et al.* (1992) Tau protein induces bundling of microtubules *in vitro*—Comparison of different tau isoforms and a tau protein-fragment. *J Neurosci Res* 33:19–29.
4. Kanai Y, Chen J, Hirokawa N (1992) Microtubule bundling by tau proteins *in vivo*—Analysis of functional domains. *EMBO J* 11:3953–3961.
5. Brandt R, Lee G (1993) Functional-organization of microtubule-associated protein-tau—Identification of regions which affect microtubule growth, nucleation, and bundle formation *in vitro*. *J Biol Chem* 268:3414–3419.
6. Gustke N, *et al.* (1994) Domains of tau-protein and interactions with microtubules. *Biochemistry* 33:9511–9522.
7. Drechsel D, Hyman A, Cobb M, Kirschner M (1992) Modulation of the dynamic instability of tubulin assembly by the microtubule-associated protein tau. *Mol Biol Cell* 3:1141–1154.
8. Trinczek B, *et al.* (1995) Domains of Tau-protein, differential phosphorylation, and dynamic instability of microtubules. *Mol Biol Cell* 6:1887–1902.
9. Goode B, *et al.* (1997) Functional interactions between the proline-rich and repeat regions of tau enhance microtubule binding and assembly. *Mol Biol Cell* 8:353–365.
10. Panda D, *et al.* (2003) Differential regulation of microtubule dynamics by three- and four-repeat tau: Implications for the onset of neurodegenerative disease. *Proc Natl Acad Sci USA* 100:9548–9553.
11. Levy SF, *et al.* (2005) Three- and four-repeat tau regulate the dynamic instability of two distinct microtubule subpopulations in qualitatively different manners—Implications for neurodegeneration. *J Biol Chem* 280:13520–13528.

12. Spillantini MG, *et al.* (1998) Mutation in the tau gene in familial multiple system tauopathy with presenile dementia. *Proc Natl Acad Sci USA* 95:7737–7741.
13. Clark L, *et al.* (1998) Pathogenic implications of mutations in the tau gene in pallido-ponto-nigral degeneration and related neurodegenerative disorders linked to chromosome 17. *Proc Natl Acad Sci USA* 95:13103–13107.
14. Hutton M, *et al.* (1998) Association of missense and 5′-splice-site mutations in tau with the inherited dementia FTDP-17. *Nature* 393:702–705.
15. Lee G, Cowan N, Kirschner M (1988) The primary structure and heterogeneity of tau-protein from mouse-brain. *Science* 239:285–288.
16. Lee G, Neve RL, Kosik KS (1989) The microtubule binding domain of tau-protein. *Neuron* 2:1615–1624.
17. Butner K, Kirschner M (1991) Tau-protein binds to microtubules through a flexible array of distributed weak sites. *J Cell Biol* 115:717–730.
18. Goode B, Feinstein S (1994) Identification of a novel microtubule-binding and assembly domain in the developmentally-regulated inter-repeat region of tau. *J Cell Biol* 124:769–782.
19. Serrano L, Montejo de Garcini E, Hernandez MA, Avila J (1985) Localization of the tubulin binding site for tau protein. *Eur J Biochem/FEBS* 153:595–600.
20. Maccioni RB, Rivas CI, Vera JC (1988) Differential interaction of synthetic peptides from the carboxyl-terminal regulatory domain of tubulin with microtubule-associated proteins. *EMBO J* 7:1957–1963.
21. Chau M, *et al.* (1998) The microtubule-associated protein tau cross-links to two distinct sites on each alpha and beta tubulin monomer via separate domains. *Biochemistry* 37:17692–17703.
22. Himmler A, Drechsel D, Kirschner MW, Martin DW (1989) Tau consists of a set of proteins with repeated C-terminal microtubule-binding domains and variable N-terminal domains. *Mol Cell Biol* 9:1381–1388.
23. Goedert M, *et al.* (1989) Multiple isoforms of human microtubule-associated protein-tau-sequences and localization in neurofibrillary tangles of Alzheimers-disease. *Neuron* 3:519–526.
24. Kosik K, Orecchio L, Bakalis S, Neve R (1989) Developmentally regulated expression of specific tau sequences. *Neuron* 2:1389–1397.
25. Goode B, Chau M, Denis P, Feinstein S (2000) Structural and functional differences between 3-repeat and 4-repeat tau isoforms—Implications for normal tau function and the onset of neurodegenerative disease. *J Biol Chem* 275:38182–38189.
26. Bunker J, Wilson L, Jordan M, Feinstein S (2004) Modulation of microtubule dynamics by tau in living cells: Implications for development and neurodegeneration. *Mol Biol Cell* 15:2720–2728.
27. Brandt R, Leger J, Lee G (1995) Interaction of tau with the neural plasma-membrane mediated by tau amino-terminal projection domain. *J Cell Biol* 131:1327–1340.
28. Sengupta A, Novak M, Grundke-Iqbal I, Iqbal K (2006) Regulation of phosphorylation of tau by cyclin-dependent kinase 5 and glycogen synthase kinase-3 at substrate level. *FEBS Lett* 580:5925–5933.
29. Cleveland D, Hwo S, Kirschner M (1977) Purification of tau, a microtubule-associated protein that induces assembly of microtubules from purified tubulin. *J Mol Biol* 116:207–225.
30. Schweers O, Schonbrunnhanebeck E, Marx A, Mandelkow E (1994) Structural studies of tau-protein and Alzheimer paired helical filaments show no evidence for beta-structure. *J Biol Chem* 269:24290–24297.
31. Ringel I, Sternlicht H (1984) C-13 nuclear magnetic-resonance study of microtubule protein—Evidence for a 2nd colchicine site involved in the inhibition of microtubule assembly. *Biochemistry* 23:5644–5653.
32. Woody RW, Roberts GCK, Clark DC, Bayley PM (1982) H-1-NMR evidence for flexibility in microtubule-associated proteins and microtubule protein oligomers. *FEBS Lett* 141:181–184.
33. Hernandez M, Avila J, Andreu J (1986) Physicochemical characterization of the heat-stable microtubule-associated protein Map2. *Eur J Biochem/FEBS* 154:41–48.
34. Black M (1987) Comparison of the effects of microtubule-associated protein-2 and tau on the packing density of *in vitro* assembled microtubules. *Proc Natl Acad Sci USA* 84:7783–7787.
35. Mukhopadhyay R, Kumar S, Hoh JH (2004) Molecular mechanisms for organizing the neuronal cytoskeleton. *BioEssays* 26:1017–1025.
36. Mukhopadhyay R, Hoh JH (2001) AFM force measurements on microtubule-associated proteins: The projection domain exerts a long-range repulsive force. *FEBS Lett* 505:374–378.
37. Marx A, Pless J, Mandelkow EM, Mandelkow E (2000) On the rigidity of the cytoskeleton: Are maps crosslinkers or spacers of microtubules? *Cell Mol Biol* 46:949–965.
38. Hirokawa N, Hisanaga S, Shiomura Y (1988) Map2 is a component of crossbridges between microtubules and neurofilaments in the neuronal cytoskeleton—Quick-freeze, deep-etch immunoelectron microscopy and reconstitution studies. *J Neurosci* 8:2769–2779.
39. Aamodt E, Culotti J (1986) Microtubules and microtubule-associated proteins from the nematode *Caenorhabditis-elegans*—Periodic cross-links connect microtubules *in vitro*. *J Cell Biol* 103:23–31.
40. Needleman DJ, *et al.* (2004) Synchrotron x-ray diffraction study of microtubules buckling and bundling under osmotic stress: A probe of interprotofilament interactions. *Phys Rev Lett* 93:198104.
41. Israelachvili J (1992) *Intermolecular and Surface Forces* (Academic, San Diego).
42. Kohn JE, *et al.* (2004) Random-coil behavior and the dimensions of chemically unfolded proteins. *Proc Natl Acad Sci USA* 101:12491–12496.
43. Shapiro L, *et al.* (1995) Structural basis of cell-cell adhesion by cadherins. *Nature* 374:327–337.
44. Chappuis-Flament S, *et al.* (2001) Multiple cadherin extracellular repeats mediate homophilic binding and adhesion. *J Cell Biol* 154:231–243.
45. Sivasankar S, *et al.* (1999) Direct molecular force measurements of multiple adhesive interactions between cadherin ectodomains. *Proc Natl Acad Sci USA* 96:11820–11824.
46. Garcia de Ancos J, Correas I, Avila J (1993) Differences in microtubule binding and self-association abilities of bovine brain tau-isoforms. *J Biol Chem* 268:7976–7982.
47. Schweers O, Mandelkow EM, Biernat J, Mandelkow E (1995) Oxidation of cysteine-322 in the repeat domain of microtubule-associated protein-tau controls the *in-vitro* assembly of paired helical filaments. *Proc Natl Acad Sci USA* 92:8463–8467.
48. Paudel HK (1997) Phosphorylation by neuronal cdc2-like protein kinase promotes dimerization of tau protein *in vitro*. *J Biol Chem* 272:28328–28334.
49. Di Noto L, DeTure M, Purich D (1999) Disulfide-cross-linked tau and MAP2 homodimers readily promote microtubule assembly. *Mol Cell Biol Res Commun* 2:71–76.
50. Makrides V, *et al.* (2003) Microtubule-dependent oligomerization of tau—Implications for physiological tau function and tauopathies. *J Biol Chem* 278:33298–33304.
51. Sahara N, *et al.* (2007) Assembly of two distinct dimers and higher-order oligomers from full-length tau. *Eur J Neurosci* 25:3020–3029.
52. Park S-Y, Ferreira A (2005) The generation of a 17 kDa neurotoxic fragment: An alternative mechanism by which tau mediates β-amyloid-induced neurodegeneration. *J Neurosci* 25:5365–5375.
53. Murphy DB, Borisy GG (1975) Association of high-molecular-weight proteins with microtubules and their role in microtubule assembly *in vitro*. *Proc Natl Acad Sci USA* 72:2696–2700.
54. Sloboda RD, Rosenbaum JL (1979) Decoration and stabilization of intact, smooth-walled microtubules with microtubule-associated proteins. *Biochemistry* 18:48–55.